Journal of Oceanography (2021) 77:17–28
https://doi.org/10.1007/s10872-020-00574-2

SPECIAL SECTION: ORIGINAL ARTICLE

Ocean Mixing Processes (OMIX): Impact on Biogeochemistry, Climate and Ecosystem

Estimate of turbulent energy dissipation rate using free-fall and CTD-attached fast-response thermistors in weak ocean turbulence

Ichiro Yasuda[1] · Shinzou Fujio[1] · Daigo Yanagimoto[1] · KeungJong Lee[1] · Yusuke Sasaki[1] · Shuo Zhai[1] · Mamoru Tanaka[1] · Sachihiko Itoh[1] · Takahiro Tanaka[2] · Daisuke Hasegawa[2] · Yasutaka Goto[3] · Daisuke Sasano[3]

Received: 14 May 2020 / Revised: 2 October 2020 / Accepted: 18 October 2020 / Published online: 5 January 2021

Abstract

The measurement of turbulence is necessary to quantify the vertical, diapycnal transport of heat, water and substances influencing climate, nutrient supply and marine ecosystems. As specialist instrumentation and ship-time are required to conduct microstructure measurements to quantify turbulence intensity, there is a need for more inexpensive and easy measurement methods. This study demonstrated that the turbulent energy dissipation rate, ε, estimated from fast-response thermistors Fastip Probe model 07 (FP07) with the depth-average of a > 10 m depth interval well agreed with those from current shear probes to a range of 10^{-11} W/kg (m^2s^{-3}) in the two casts of the most accurate and stable free-fall vertical microstructure profiler, VMP6000 in the Oyashio water. This range cannot be measured with velocity shear probes equipped in smaller profilers in which the lower limit of $\varepsilon > O(10^{-10})$ W/kg. These results extend turbulence measurements using the FP07 to 10^{-11} W/kg. They may be especially useful for turbulence observations in deep oceans where ε is generally weak ($< 10^{-10}$ W/kg). As FP07 are much less sensitive to instrument vibrations than current shear and may be attached to various observational platforms such as temperature-conductivity-depth (CTD) profilers and floats. The CTD-attached FP07 observations near the VMP6000 profiles demonstrated their capabilities in the ε range of 10^{-11}–10^{-8} W/kg by data screening using a $W_{sd} > 0.1(W - 0.3)$ criterion (1 s mean lowering rate W m/s and its standard deviation W_{sd}) under rough conditions where the cast-mean $W_{sd} >$ 0.07 m/s and the standard deviation of W_{sd} in each cast $\sigma > 0.05$ m/s.

Keywords Turbulence · Turbulent energy dissipation · Deep ocean · Microstructure · CTD-attached fast-response thermistor

1 Introduction

The measurement of ocean turbulence is necessary to quantify the vertical, diapycnal transport of heat, water (Munk 1966; Bryan 1987; Oka and Niwa 2013), and substances that control climate (Yasuda et al. 2006; Hasumi et al. 2008; Yasuda 2009, 2018; Tanaka et al. 2012a, b; Tatebe et al. 2018; Watanabe et al. 2020), nutrient supply (Tanaka et al. 2012a, b; Kaneko et al. 2013; Nishioka et al. 2020; Tanaka et al. 2020) and marine ecosystems (e.g. Kobari et al. 2020). As specialist instrumentation and ship-time are required to conduct microstructure turbulence measurements, there is a need to develop more efficient measurement methods. This study attempts to utilise the fast-response thermistor FP07 (Fastip Probe model 07) to observe turbulence in deep oceans where turbulence represented by the turbulent energy dissipation rate, ε, is generally too weak ($\varepsilon < 10^{-10}$ W/kg) to be measured using micro-scale current shear probes that are typically used for turbulence measurements. ε exhibits 4 orders of magnitude variability in the deep ocean with elevated $\varepsilon \sim O(10^{-8})$ W/kg in limited areas over rough bottom topography (e.g. Waterhouse et al. 2015; Goto et al. 2020).

Turbulence measurements using fast-response thermistors were developed and had commenced in the 1970s (Cox et al. 1969; Gregg et al. 1978). Using temperature

✉ Ichiro Yasuda
ichiro@aori.u-tokyo.ac.jp

[1] Atmosphere and Ocean Research Institute, The University of Tokyo, Kashiwa, Chiba, Japan

[2] Fisheries Resources Institute, Japan Fisheries Research and Education Agency, Shiogama, Miyagi, Japan

[3] Japan Meteorological Agency, Tokyo, Japan

gradient—wavenumber spectra, the FP07 measurements yield not only ε but also thermal dissipation rate χ (Oakey 1982), both of which give vertical diffusivity (Osborn 1980; Osborn and Cox 1972). However, the FP07 measurements have been much less common as the temporal response of these sensors were not sufficient for strong turbulence environment and individual sensors have different response (Lueck et al. 1977; Gregg and Meagher 1980; Oakey 1982; Gregg 1999). Since ε is directly computed from velocity microstructure, shear probes with manufacture's calibration have commonly been used to measure ε in recent years, especially for shallow waters with relatively strong turbulence. Horizontal profiling of towed bodies or submarines with shear probes were conducted in the 1980s (Lueck et al. 2002).

Whereas, since the shear probe measurements that observe micro-scale water vibrations are very sensitive to instrument vibrations, the shear probe measurements of weak turbulence in deep oceans require stable and free-fall (or free-rise) platforms and a large length of instruments to resolve vortex motions with relatively large O(10^{-1}–10^{0} m) length scale which contributes to weak turbulence. In contrast, the FP07 is much less sensitive to instrument vibration as it measures micro-scale water temperature variability, and can be attached to various observational platforms such as moorings (Moum and Nash 2009; Becherer and Moum, 2017). The FP07 is also good at measuring relatively low-wavenumber (thus relatively large length scale) signal which is not attenuated by the insufficient temporal response to cause a decay of the high-wavenumber part of the temperature spectra and to underestimate strong turbulence.

To improve the FP07 measurements, correction methods to compensate for the insufficient temporal response have been elaborated (Lueck et al. 1977; Gregg and Meagher 1980; Oakey 1982; Gregg 1999). Goto, Yasuda and Nagasawa (2016, henceforth GYN16) confirmed it effective to use a method ('double pole function with a time constant of 3 ms' as will be described in the next section) as well as to use a spectrum fitting procedure (Ruddick et al. 2000; Peterson and Fer 2014) by performing simultaneous shear-probe and FP07 free-fall measurements, and ε range of 10^{-10}–3×10^{-7} W/kg was confirmed to be measured with the free-fall FP07.

To extend the FP07 measurements to 'not-free-fall' FP07 attached to common oceanographic temperature-salinity-depth (CTD) observation platforms, data screening methods to reject bad data were developed, and an ε range between 10^{-10}–10^{-8} W/kg was confirmed to be reasonably measured by comparing the not-free-fall CTD-attached FP07 with the quasi-simultaneous free-fall measurements at the same locations within a few hours of each other (Goto, Yasuda and Nagasawa 2018; henceforth GYN18).

This study attempts to extend the lower limit of the FP07 measurements to $\varepsilon \sim$ O(10^{-11}) W/kg which enables to cover most of the deep oceans. Since the lower limit $\varepsilon \sim 10^{-10}$ W/kg of the previous measurements (GYN16; GYN18) is not the limit of the FP07 but the limit of the previous shear probe measurements by free-fall but tethered VMP2000 (Rockland Sci.) in GYN16 and GYN18, we here used a higher-accuracy shear and FP07 measurements using the free-fall (untethered, larger and stable) vertical microstructure profiler (VMP6000; Rockland Scientific). Firstly, the extension to the $\varepsilon \sim 10^{-11}$ W/kg limit was successful for the simultaneous shear and FP07 measurements on the free-fall VMP6000. Similar attempts were independently performed with a glider with shear and FP07 (Sheifele et al. 2018) which confirmed the validity down to 3×10^{-11} W/kg in the relatively shallow water (< 400 m). The reliable free-fall VMP6000 will confirm the validity of FP07 in deep water.

Then, two pairs of CTD-attached FP07 and quasi-simultaneous free-fall VMP6000 shear measurements were compared to evaluate the availability of the CTD-attached FP07 measurements. For reasonable CTD-attached FP07 observations, some modification for the data screening method (GYN18) was required for rough sea-state and/or winch trouble which caused large lowering speed variability and large vibrations.

2 Data and methods

Two pairs of casts of the VMP6000 and the CTD with FP07 were conducted in the cruise of the R/V Shinsei-Maru (belonging to the Japan Agency for Marine-Earth Science and Technology), between April 19–28, 2019. The deployment and recovery of these casts are listed in Table 1. Figure 1 depicted the two pairs of the temperature vertical profiles at the stations FL2 and C04 with the VMP6000 (Rockland Scientific) and CTD (SeaBird 9plus) which were conducted quasi-simultaneously within 1 h and showed similar temperature profiles.

The VMP6000 is recognized as the most accurate free-fall vertical microstructure profiler with two fast-response thermistors (FP07), two velocity shear probes and the SeaBird pumped (SBE5T)- temperature (SBE3F) and conductivity (SBE4C) sensors. Assuming isotropic turbulence, measuring the vertical shear of horizontal velocity $\frac{\partial u'}{\partial z}$ in the scale of O(10^{-2}–10^{0} m), which is obtained using velocity shear probes, enables the computation of the turbulent energy dissipation rate: $\varepsilon = \frac{15}{2}\nu\overline{\left(\frac{\partial u'}{\partial z}\right)^2}$ where ν is the kinematic viscosity. VMP6000 can measure ε in the range of O(10^{-11}–10^{-5})W/kg. In this study, raw shear data were sampled at 512 Hz, and Fast Fourier Transform (FFT) frequency spectra were computed at every 2 s (1024 data points) after

Table 1 List of observation stations (Stn), instrument items, action, date, time, latitude, longitude and bottom depth in the KS-19–6 cruise of the R/V Shinsei-Maru

Stn	Item	action	Date UTC	Time	Longitude	Latitude	Depth (m)
FL2	VMP6000	Release	2019/4/21	19:30	143–40.5342°E	40–27.9884°N	2748
FL2	VMP6000	Recover	2019/4/21	22:25	143–39.9629°E	40–28.1837°N	2681
FL2	CTD/FP07	Start	2019/4/21	19:45	143–40.7163°E	40–27.7878°N	2780
FL2	CTD/FP07	Bottom	2019/4/21	20:48	143–40.7366°E	40–27.9603°N	2772
FL2	CTD/FP07	End	2019/4/21	21:59	143–40.6276°E	40–28.3768°N	2740
C04	VMP6000	Release	2019/4/22	21:38	144–50.7213°E	39–59.5594°N	5830
C04	VMP6000	Recover	2019/4/23	4:00	144–50.9118°E	40–0.0103°N	5816
C04	CTD/FP07	Start	2019/4/22	21:58	144–50.3905°E	39–59.9644°N	5838
C04	CTD/FP07	Bottom	2019/4/23	0:28	144–50.4689°E	39–59.7527°N	5835
C04	CTD/FP07	End	2019/4/23	3:42	144–50.8021°E	39–59.913°N	5822

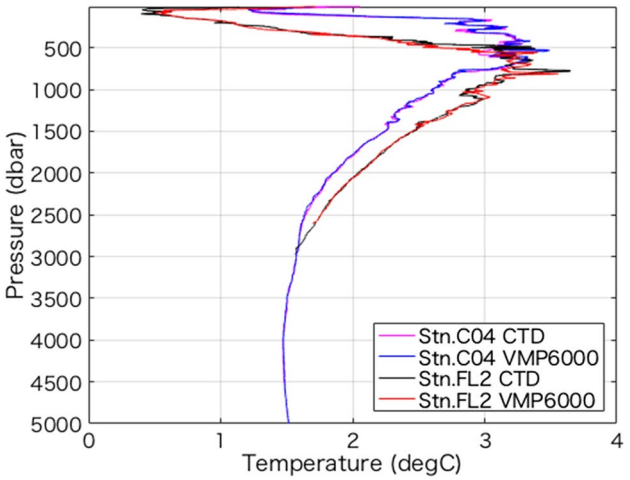

Fig. 1 Vertical temperature (°C) profiles of VMP6000 (red) and CTD (black) at Stn. FL2, and VMP6000 (cyan) and CTD (blue) at Stn. C04 (colour figure online)

removing the noise of the instrument using acceleration sensors equipped with a profiler (Lueck et al. 2002; Goodman et al. 2006). Then ensemble mean spectra were computed from 4 spectra during 8 s. The frequency spectra were then converted to wavenumber (in cpm) spectra using the vertical fall rate of the profiler, assuming Taylor's frozen turbulence hypothesis. As such, ε was derived by integrating the wavenumber spectrum from the lowest wavenumber to the Kolmogorov wavenumber $k_\nu = (\varepsilon/\nu^3)^{1/4}/(2\pi)$. This procedure yields dissipation rates every 8 s with half overlap; that is, 8-s mean ε every 4 s.

ε is also estimated using the temperature microstructure FP07 data under the assumption of isotropic turbulence. In this method, the Kraichnan (1968) universal spectrum is fitted to the observed temperature gradient spectrum with a maximum likelihood method (Ruddick et al., 2000) and discarding the ill-shaped spectrum with certain parameters based on Peterson and Fer's (2014) criteria. Then, the Batchelor wavenumber $k_\mathrm{B} = (\varepsilon/(\nu\kappa^2))^{\frac{1}{4}}/(2\pi)$ (Batchelor 1959) is detected via detecting the wavenumber at the spectrum peak $k_\mathrm{P}(= k_B(6q_\mathrm{K})^{-\frac{1}{2}})$ where the Kraichnan constant, q_K, is set at 5.26 (Bogucki et al. 1997; 2012) (see Appendix Fig. 9 for the ε estimation from FP07 based on the spectra and fitting procedures). This Batchelor wavenumber yields turbulent energy dissipation rate $\varepsilon = \nu\kappa^2(2\pi k_\mathrm{B})^4$, which relies on the detection of $k_\mathrm{P}(\propto \varepsilon^{1/4})$ and the spectrum fitting. For the seawater with the large Prandtl number $(= \nu/\kappa)$, $k_\mathrm{B} \gg k_\nu$, and we thus use the temperature gradient spectra in the wider wavenumber ranges from viscous-convective to viscous-diffusive regimes than for the velocity-shear spectra (e.g. Becherer and Moum 2017 which used lower wavenumber range from inertial-convective to viscous-convective regimes). The temporal response of FP07 is insufficient under strong turbulence for $\varepsilon > 10^{-9}$ W/kg under the instrument lowering speed of $W \sim 0.7$ m/s (GYN16), and correction to the frequency f domain are required (Lueck et al. 1997). A correction of the double pole function $[1 + (2\pi f\tau)^2]^2$ (Gregg and Meagher 1980; Gregg 1999) to frequency spectra with a time constant τ of 3 ms was operated (GYN16). For the VMP6000 with nearly constant $W \sim 0.7$ m/s, the 8 s FP07 data with the sampling rate at 512 Hz was used to create the temperature gradient spectra. For the relatively weak turbulence range of $\varepsilon < 10^{-9}$ W/kg, GYN16 has confirmed that ε measurements with FP07 are independent of the correction and the time constant by comparing with shear probe measurements. The FP07 and pressure data were recorded with the efficient data sampling and deconvolution method (Lueck and Mudge 1994).

For the CTD-attached FP07 measurements, the AFP07 system (Rockland Scientific) composed of a data-logger and two separated FP07 sensors, was attached to a CTD-frame. The power of this AFP07 was supplied from the SeaBird 9plus CTD, and the temperature data was also supplied from the CTD to calibrate FP07 data and recorded in the data-logger together with the FP07 temperature, acceleration and pressure data. The FP07 and acceleration data were sampled at 512 Hz, the pressure data at 64 Hz.

Data processing for the CTD-attached FP07 is almost the same as for the FP07 of the VMP6000 measurements, except for a few things. One difference is that the FFT-length is set at 1 s for computing temperature gradient spectra due to large variability of CTD lowering speed W because the CTD is connected to ship with steel cable and the rolling and pitching of the ship directly affects W. Constant W is assumed in the Taylor's frozen turbulence hypothesis, and FFT-length is required as short as possible not to violate the hypothesis, whereas 1 s is necessary to resolve 1 m length scale for the standard CTD lowering speed $W \sim 1$ m/s. Another difference is the time constant of the CTD-attached FP07 used; 1.5 ms was set to make the ratio $\varepsilon_{TC}/\varepsilon_S \sim 1$ (ε_{TC} from CTD-attached FP07 and ε_S from the shear probe on the VMP6000). In addition, the rejection of abnormal data was required for the not-free-fall CTD-attached FP07 despite it being much less sensitive to instrument vibration than the velocity shear probe measurement. GYN18 compared ε_{TC} from CTD-attached FP07 with ε_S from quasi-simultaneous free-fall VMP2000 shear, where the FP07 measurements were undertaken within a few hours of each other. They proposed the rejection of data when $W_{sd} > 0.2(W - 0.3)$, where W_{sd} and W (in m/s) were the standard deviation and mean of the lowering speed of each 1 s data, computed from pressure data sampled at 64 Hz. Based on this criterion, data for the slow lowering speed $W < 0.3$ m/s, or for the large speed variability $W_{sd} > 0.14$ m/s (assuming the standard lowering speed of 1 m/s) is always rejected. As such, W_{sd} is a means to evaluate the cast condition because the conditions of sea-state or of winch directly affect W_{sd} through the cable which connects between CTD and ship. Cast-mean W_{sd}, standard deviation σ of W_{sd} in each cast and cast-mean $W_{sd}+\sigma$ are used as parameters to represent the observational condition as shown in Table 2 and Fig. 7 where the data was obtained in the RF-16–6 Ryofu-Maru belonging to the Japan Meteorological Agency (JMA) from July 3 to August 24, 2016. In addition to this data screening, data at the minimum W were also rejected following Goto (2018) and Goto et al. (2020).

Table 2 List of cast-mean standard deviation W_{sd} (in m/s) of each CTD-cast (mean-W_{sd}), the standard deviation σ of the W_{sd} in each cast and mean-$W_{sd}+\sigma$ at each CTD station in various cruises

Station	Cruise	mean-W_{sd}	Std (W_{sd}):σ	mean-$W_{sd}+\sigma$
C04	KS-19–6	0.0704	0.0518	0.1222
FL2	KS-19–6	0.0664	0.0454	0.1118
278_006	KS-18–5	0.015	0.0197	0.0347
178_816	JMA	0.0444	0.0311	0.0755

3 Results

3.1 Extend FP07 ε estimate to O(10^{-11}) W/kg by comparing with simultaneous shear measurements on a free-fall VMP6000

Comparison of ε on the VMP6000 data demonstrated that ε_{T6} estimated from the FP07 was as accurate as ε_S from the velocity shear probe, even for the weak turbulence range to $\varepsilon \sim$ O(10^{-11})W/kg as shown in Fig. 2a at Station FL2. In this figure, the 50 m depth averaged profiles for the FP07 represented by the red line, and the blue line for velocity shear are in good agreement within a 95% confidence level, as represented by the shades estimated using the bootstrap method. Whereas, the raw data (roughly 5 m depth bin from 8 s) denoted by the dots were scattered, especially for ε_{T6}. It was confirmed that the lower limit of ε_S reached 10^{-11} W/kg for raw ε_S and even for the 50 m averaged ε_S at Station C04 (Fig. 6a). This extends the lower detection limit of ε_{T6} from the FP07 to 10^{-11} W/kg from 10^{-10} W/kg in the previous studies (GYN16; GYN18) where instruments (tethered and smaller VMP2000, Rockland Scientific) with less accurate profiles, reliable only for $\varepsilon_S > 10^{-10}$ W/kg, were used.

This agreement between ε_{T6} and ε_S from the free-fall VMP6000 data was also confirmed for the 10 m depth-averaged data, shown in the scatter plot for Station FL2 (dots in Fig. 2b) as well as for the 50 m depth mean (red circles in Fig. 2b). The 10 m mean data were somewhat scattered, mostly within a factor of three. This is considered reasonable as even ε_S from the two shear probes which were closely (< 10 cm) located and simultaneously measured were scattered similarly (GYN16). The 10 m mean $\log_{10}(\varepsilon_{T6}/\varepsilon_S)$ plot and the mean at each ε_S range (Fig. 2c) also confirm the validity of ε_{T6} to 10^{-11} W/kg.

The wavenumber spectra of the velocity shear and temperature gradient of VMP6000 were confirmed to be reasonable for $O(10^{-11}) \leq \varepsilon_{T6} \leq O(10^{-9})$ W/kg as shown in the upper and middle panels of Fig. 3 where the spectrum amplitude was averaged at each wavenumber in each order of ε_{T6}. The observed mean shear spectra well followed the Nasmyth (1970) universal spectrum (red curve in upper panels). The observed temperature gradient spectra of VMP6000 (middle panels in Fig. 3) were well resolved around the peaks of the spectra which were well fitted to the Kraichnan (1968) universal spectrum (red curves in middle panels) to yield reasonable Batchelor wavenumber and ε_{T6}. It is noted that the shear spectra in $O(10^{-13}) - O(10^{-12})$ (a and b of upper panels) are similar to the one in $O(10^{-11})$ and the mean $\varepsilon_S \gg \varepsilon_{T6}$ as in the numerical values on the upper-left corner whereas the temperature gradient spectra do change. This suggests that the lower limit of shear measurements is $O(10^{-11})$ W/kg and FP07 measurements extend to further lower.

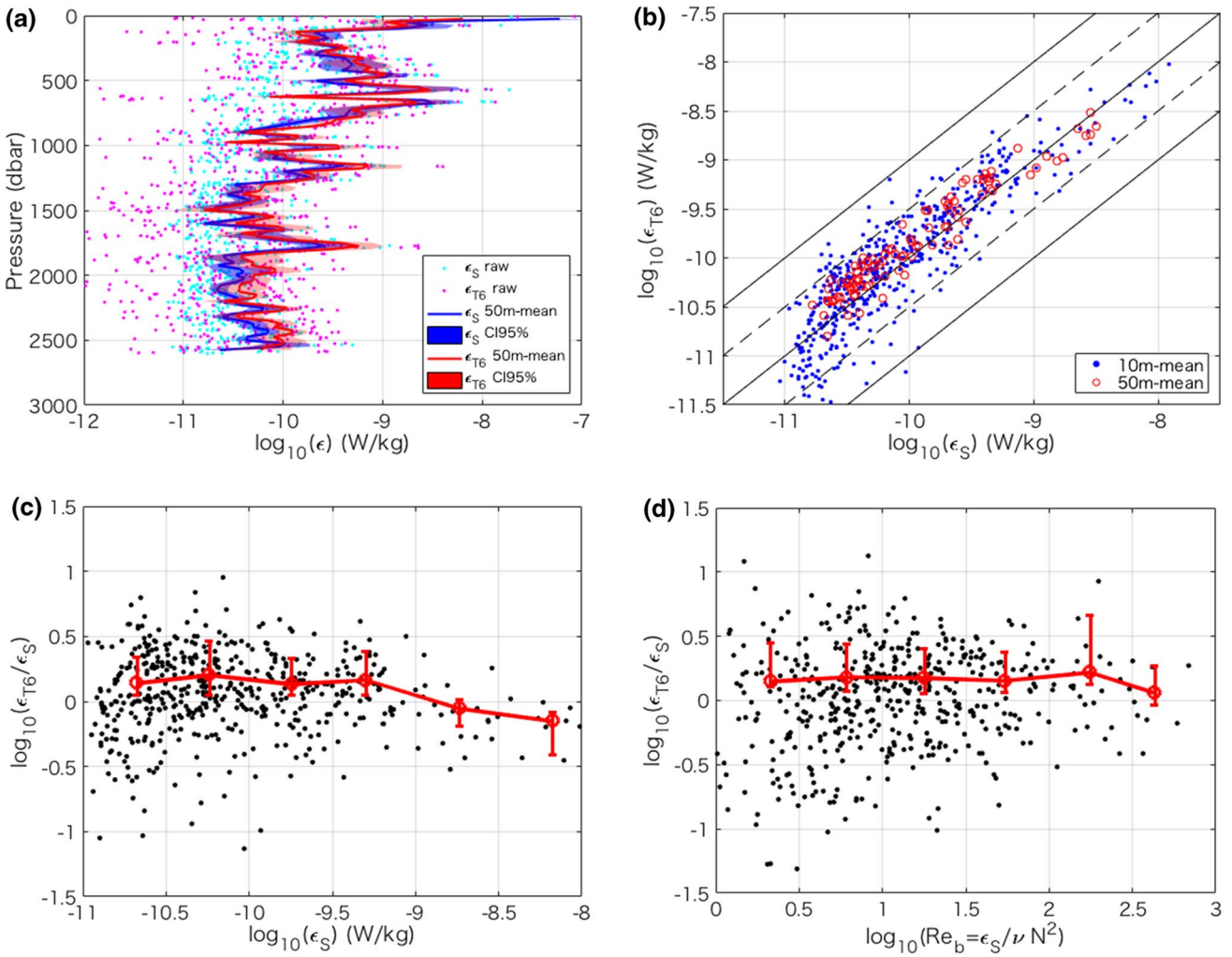

Fig. 2 **a** Vertical profiles of turbulent energy dissipation rate ε at Stn. FL2. ε_S from shear (blue dots: raw data, blue line: 50 m depth mean and blue shades: 95% confidence interval of the 50 m depth mean) and ε_{T6} from FP07 (same as shear except in red dots, line and shades) measured simultaneously by free-fall VMP6000 at Station FL2; **b** scatter plot of ε_S versus ε_{T6} on VMP6000 (blue dots: 10 m mean, red circles: 50 m mean, solid lines: $Y=X$ and $Y=X\pm1$, broken lines: $Y=X\pm0.5$); **c** dependence of 10 m mean $\log_{10}(\varepsilon_{T6}/\varepsilon_S)$ on ε_S (black dots) and 0.5-$\log_{10}(\varepsilon_S)$-mean $\log_{10}(\varepsilon_{T6}/\varepsilon_S)$ (red circles) and 95% confidence interval (red error bars). **d** Same as **c** but for the dependence on the Buoyancy Reynolds number $R_{eB}=\varepsilon_S/\nu N^2$ at Stn. FL2 and C04 (colour figure online)

The histograms of ε_S (Fig. 4a) and ε_{T6} (Fig. 4b) also confirm that the lower limit of $\varepsilon_S\sim 10^{-11}$ W/kg with cut-off there (gray bars in Fig. 4a) and the lower limit of ε_{T6} extends further lower with keeping log-normal distribution (Fig. 4b). Similar results were reported by Sheifele et al. (2018) on the basis of microstructure data from glider observations. It is also noted that 10 m-mean (cyan in Fig. 4a) and 50 m-mean (red in Fig. 4a) ε_S distributions approach to log-normal and the 10 m-mean and 50 m-mean statistics such as mode, median and average are very similar between ε_S and ε_{T6}, supporting the consistency shown in Fig. 2.

We here discuss the consistency of shear-derived ε_S and FP07-derived ε_{T6} in the low Buoyancy Reynolds Number $R_{eB}(=\frac{\varepsilon}{\nu N^2}=\left(\frac{l_o}{l_\nu}\right)^{4/3})$ where $l_o(=\varepsilon^{1/2}N^{-2/3})$ is Ozmidov (1965) -scale representing the largest turbulent eddies under stratification and the Kolmogorov viscous scale $l_\nu=(\varepsilon/\nu^3)^{-1/4}$, and R_{eB} represents a measure of isotropy (Gargett et al. 1984): isotropic assumption is expected for $R_{eB}>100$, for $R_{eB}\sim O(10)$ anisotropy emerges but ε_S from vertical shear of turbulent velocity under the assumption of isotropy is greater by at most 35% than the true value (Yamazaki and Osborn 1990), and for R_{eB}<O(1) anisotropic turbulence regime is further prevalent.

As shown in Fig. 2d, FP07-derived ε_{T6} is consistent with shear-derived ε_S for a wide range of $R_{eB}\sim O(1-100)$, indicating that FP07-derived ε_T is reliable for $R_{eB}>O(10)$ (Yamazaki and Osborn 1990). It is noted that the normalized temperature gradient spectra (lower panels of Fig. 5, Dillon and Caldwell 1980) is consistent with the Kraichnan (1968)

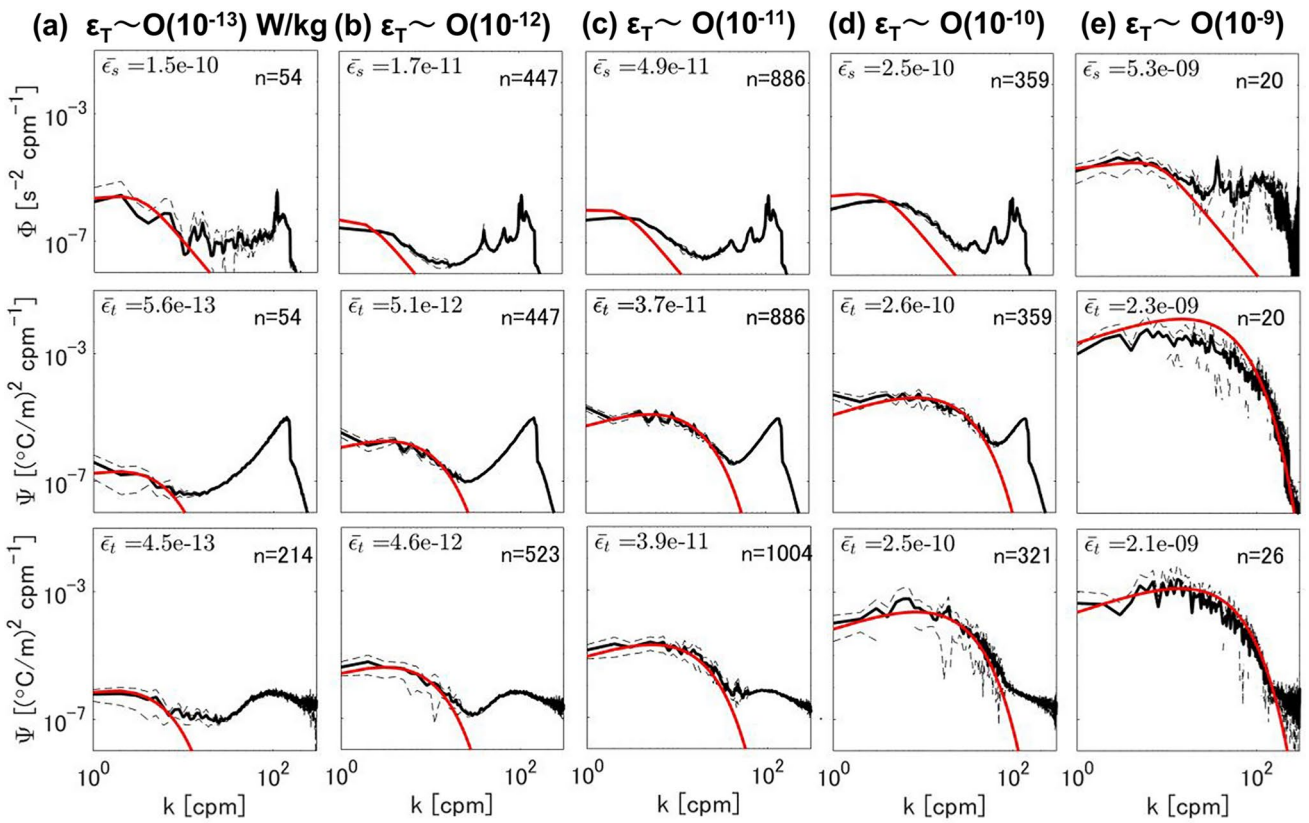

Fig. 3 Mean wavenumber spectra (thick curves) where amplitude at each wavenumber is averaged, 95% confidence intervals (broken curves) and mean universal spectra (red curves) of velocity shear Φ (upper panels), temperature gradient Ψ on VMP6000 (middle) and temperature gradient Ψ from CTD-attached FP07 (lower) in each order from O(10^{-13}) to O(10^{-9}) W/kg of turbulent energy dissipation rate ε_T from FP07 on VMP6000 for the upper (shear) and middle panels and from CTD-attached FP07 for the lower panels at Station FL2. The universal spectra are Nasmyth (1970) spectrum for Φ and Kraichnan (1968) spectrum for Ψ. The numerals on the upper-left and upper-right corners are the mean dissipation rates (in W/kg) estimated from each method and number of spectra. Spectra were composed of data after rejecting all the criteria described in Sect. 2 (colour figure online)

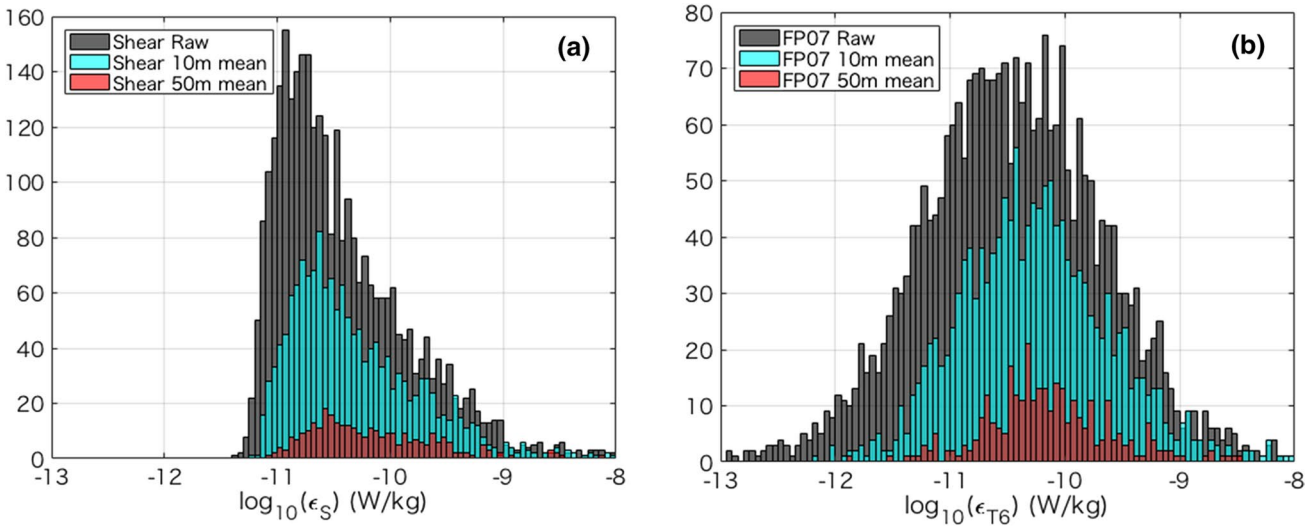

Fig. 4 Histogram of the turbulent energy dissipation rate **a** ε_S from shear and **b** ε_{T6} from FP07 on VMP6000 at Stns. FL2 and C04. The gray, cyan and red bars denote raw (8 s), 10 m mean and 50 m mean data, respectively (colour figure online)

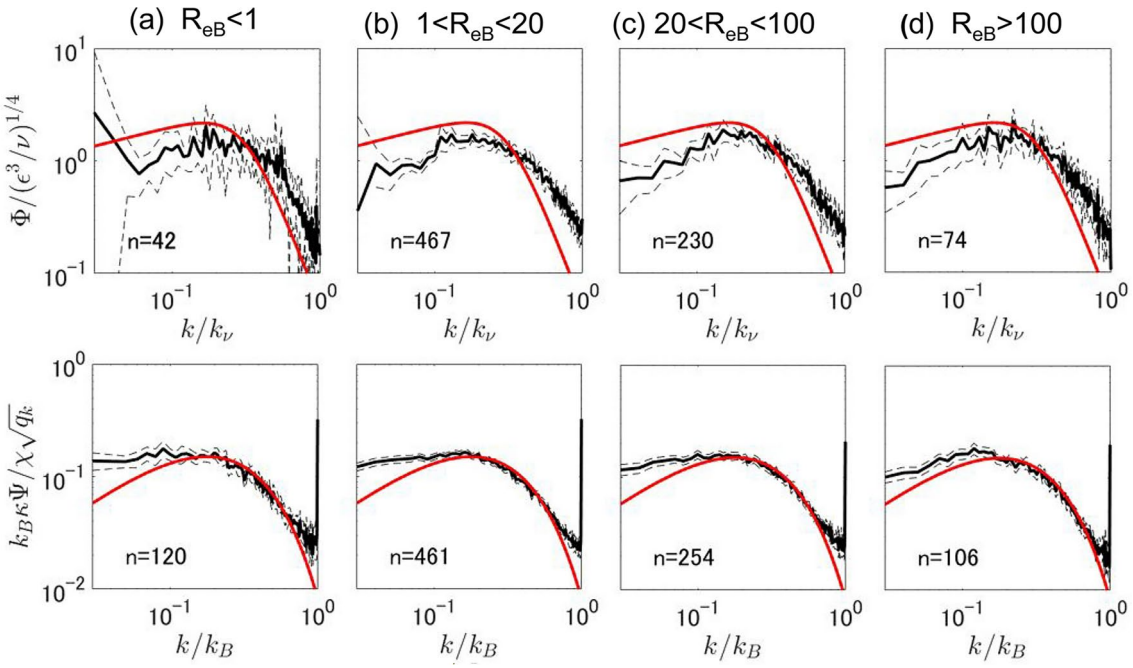

Fig. 5 Same as Fig. 3 but for showing the dependence on Buoyancy Reynolds number $R_{eB} = \frac{(\varepsilon_S, \varepsilon_{T6})}{\nu N^2}$ **a** $R_{eB} < 1$, **b** $1 < R_{eB} < 20$, **c** $20 < R_{eB} < 100$ and **d** $R_{eB} > 100$ of the mean normalized spectra of VMP6000 at Stn. FL2. For shear spectra Φ normalized by $(\varepsilon_S^3/\nu)^{1/4}$ (upper panels), the wavenumber was normalized by the Kolmogorov wavenumber $k_\nu = (\varepsilon/\nu^3)^{1/4}/(2\pi)$. For temperature gradient spectra Ψ normalized by $\chi\sqrt{q_K}/k_B\kappa$(lower panels), the wavenumber was normalized by Batchelor wavenumber $k_B = (\varepsilon_{T6}/(\nu\kappa^2))^{\frac{1}{4}}/(2\pi)$

universal spectrum derived under isotropic turbulence even for the anisotropic range of $R_{eB} < 100$ with increasing deviation (larger spectrum amplitude than the universal spectrum) in the normalized wavenumber ($k/k_B < 10^{-1}$) with less R_{eB} as also shown in Sheifele et al. (2018) in the data observed by gliders. It is also noted that the normalized shear spectra (Fig. 5 upper panels) keep the shape of the Nasmyth (1970) universal spectra in those low R_{eB}.There is still a significant amount (about 5/8 at Stn. FL2) of data with $R_{eB} < 10$ where we need to be elaborated how ε is estimated in the near future.

3.2 Evaluate ε_{TC} from not-free-fall CTD-attached FP07 by comparison with ε_S from quasi-simultaneous free-fall VMP6000

It was confirmed that the ε_{TC} vertical profile from the not-free-fall CTD-attached FP07 was similar to the ε_S from the VMP6000, measured near the CTD Sta. FL2 (Fig. 6a). As the CTD and VMP6000 casts had been separately conducted within 0.7 miles and 1.5 h at Station FL2 (Table 1), perfect agreement of the data was not expected. A comparison of ε_{TC} from CTD-attached FP07 with ε_S in the plot (Fig. 6b) shows that they show greater scattering than the data in Fig. 2b. However, the majority of the data were along the $Y = X$ line and within $Y = X \pm 1$ for the 10 m-depth mean and within $Y = X \pm 0.5$ for the 50 m-depth mean data, suggesting consistency. The composite temperature gradient spectra of the CTD-attached FP07 in each ε_{TC} order were shown to be well fitted to the Kraichnan (1968) universal spectrum for ε_{TC} of O(10^{-13}–10^{-9}) W/kg (lower panels in Fig. 3).

For this type of quasi-simultaneous comparison, some statistics were used to evaluate consistency. The standard deviation of the 10 m (50 m) depth-averaged $\log_{10}(\varepsilon_{TC}/\varepsilon_S)$ was 0.69 (0.47) at Station FL2. This is less than the log-normal standard deviation 0.96 (0.61) (Fig. 9 in GYN18 in Appendix), as the consecutive free-fall VMP shear measurements were at the same location and taken within 2 h of each other. This suggests that the ε_{TC} vertical profile from the not-free-fall CTD-attached FP07 at Station FL2 was consistent with the VMP6000 cast.

In contrast, the vertical profile of the CTD-attached ε_{TC} at Station C04 was not necessarily consistent with the ε_S from the VMP6000, as shown in Fig. 7b. Here, the ε_{TC} was at times overestimated for depths between the water surface to 2500 m. The standard deviation of the 50 m depth averaged $\log_{10}(\varepsilon_{TC}/\varepsilon_S)$ was 0.67, which is greater than 0.61 (GYN18), while the standard deviation for the 10 m mean (0.72) was less than 0.96. This overestimation may be attributed to issues with the winch system and rough sea-state, where the cable feeding system to maintain a constant speed was not used due to rough sea condition and instrument vibrations were exceptionally large, as shown in Table 2. In this instance, the cast-mean W_{sd} (mean-W_{sd}) and standard

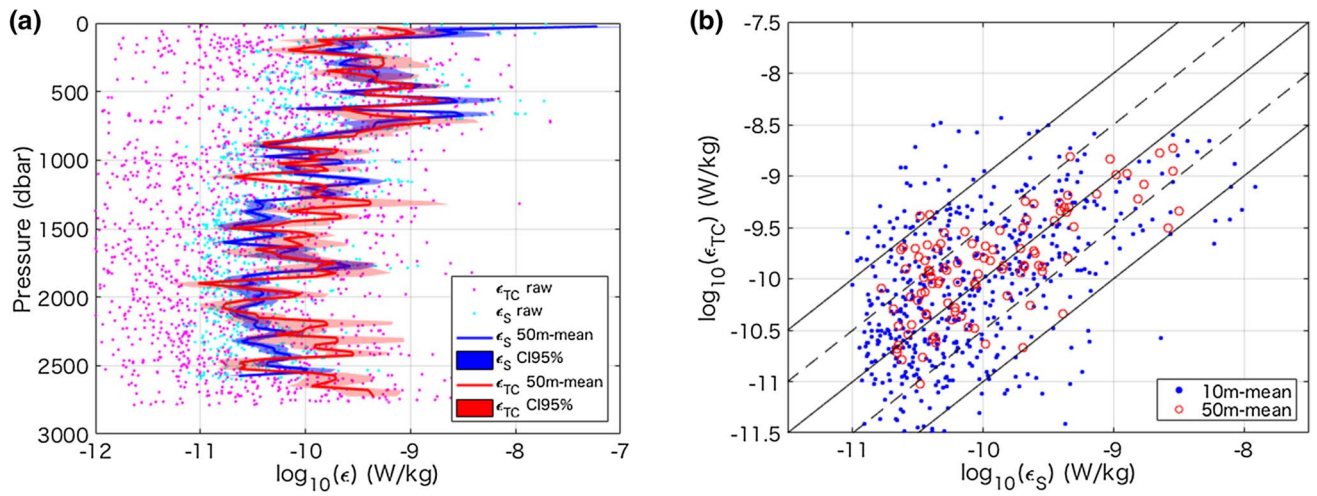

Fig. 6 Same as Fig. 2ab but for the FP07 attached to the CTD

deviation σ of W_{sd} in this cast were the largest in Table 2, while those for the KS-18–5 cruise data of the same vessel with a constant feeding winch was used (Table 2). The mean-W_{sd} and mean-$W_{sd}+\sigma$ (0.066 and 0.111) at Station FL2 were slightly lower than those at Station C04 (0.070 and 0.122) where the sea-state had been worse than at Station FL2. Such large W_{sd} as a result of the winch issue and sea-state condition may result in an inappropriate CTD-attached ε_{TC} estimation.

Further strict data screening criteria $W_{sd} > 0.1(W - 0.4)$ (Table 2 in GYN18) had effectively excluded overestimated data and rejected a greater amount of raw data (rejection rate increased from 43 to 70%, Table 3b–e), improving the correspondence between the CTD-attached ε_{TC} and ε_S (Fig. 7c). This was where the overestimated data in the upper 2500 m was largely rejected and the standard deviation of the 50 m depth averaged $\log_{10}(\varepsilon_{TC}/\varepsilon_S)$ had improved at 0.61, equivalent to the standard value of 0.61 (GYN18). This suggests that this strict rejection criterion may be appropriate for severe observational conditions, as was experienced at Station C04.

4 Discussion

The data screening criterion for the CTD-lowering rate [i.e., $W_{sd} > 0.2(W - 0.3)$ in GYN18] to choose reasonable ε_{TC} data from the CTD-attached FP07 appears to be insufficient in the situations under rough sea conditions and/or large lowering speed variability at Station C04. As such, we discuss the selection of appropriate criteria under such rough conditions. The lowering speed variability W_{sd}, may be an important parameter representing the roughness conditions (sea-state and/or winch), as derived from pressure measurements. The cast-mean W_{sd} and the standard deviation σ of W_{sd} in each cast are shown in Fig. 8, to know how variable under various sea-states. These 91 CTD cast data to the bottom along 137°E were taken in the JMA-RF-16–06 cruise with the CTD observational system (heave motion winch). The mean-W_{sd} and mean-$W_{sd}+\sigma$ was the largest (0.068, 0.116) at Station 1. These were comparable to the values at Station FL2 and were slightly lower than at Station C04 (Table 2). As that ε_{TC} vertical profile from the CTD-attached FP07 was reasonable at Station FL2, the GYN18 criterion $W_{sd} > 0.2(W - 0.3)$, may be used for the JMA CTD observations. As a practical threshold, the cast-mean $W_{sd}\sim 0.07$ and $W_{sd}+\sigma\sim 0.12$ are useful in helping to select whether the GYN18 criteria or further strict criteria should be applied. However, only two casts may be insufficient to determine this selection, and this threshold would need to be addressed in a future study.

We also discuss the criteria that are appropriate under rough conditions as experienced at Station C04. Table 3 shows the list of criteria using (W_{sd} and W) and performance represented by the rate of overestimated data ($\log_{10}(\varepsilon_{TC}/\varepsilon_S) > 1$, i.e. $(\varepsilon_{TC}/\varepsilon_S) > 10$) and the standard deviation of $\log_{10}(\varepsilon_{TC}/\varepsilon_S)$ (which should be < 0.96 for 10 m mean and < 0.61 for 50 m mean based on GYN18). Without this criterion (Table 3a), almost half (70%) of the total data for the 10 m (50 m) mean were overestimated. For the GYN18 criteria (Table 3b), 13 (9) % of the data were overestimated for the 10 m (50 m) mean. For the $W_{sd} > 0.1(W - 0.3)$ criterion (Table 3d), the overestimation had greatly reduced to 9.7 (2.9) % for the 10 m (50 m) mean, which was almost equivalent to the outcomes using the stricter criterion $W_{sd} > 0.1(W - 0.4)$ (Table 3e). The rejection rate of the raw data had lowered to 64% (Table 3d) compared to 70% (Table 3e). Due to the similar reduction of overestimated

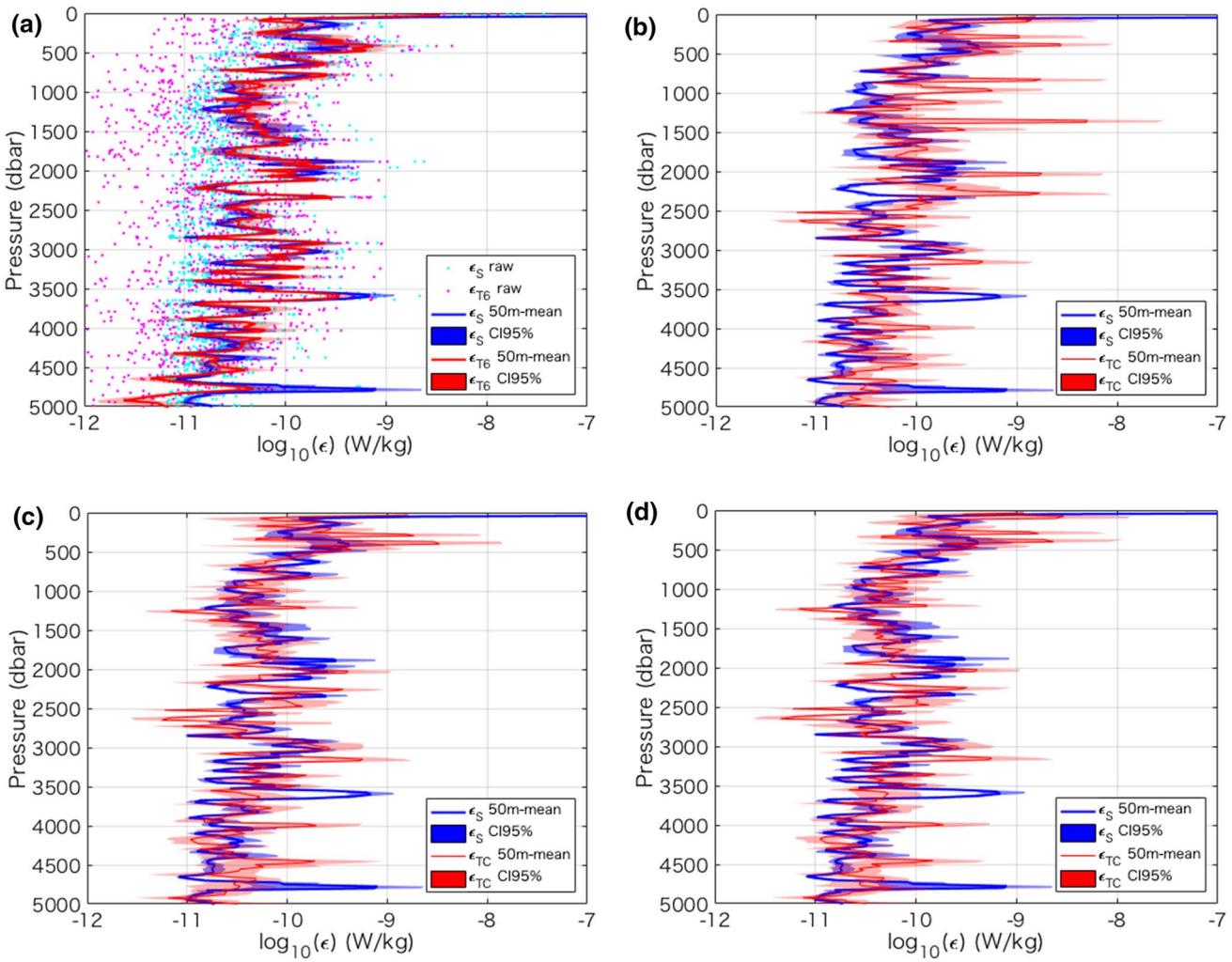

Fig. 7 **a** Same as Fig. 2a but for Station C04; **b** vertical profile of ε_S from the shear of VMP6000 at Station C04 (blue line: 50 m depth mean and blue shades: 95% confidence interval of the 50 m depth mean) and ε_{TC} from quasi-simultaneously measured FP07 attached to CTD (same as shear except using red line and shades) with the data rejection criterion $W_{sd} > 0.2(W - 0.3)$; **c** same as **b** but for the data rejection criterion $W_{sd} > 0.1(W - 0.4)$; **d** same as **b** but for the data rejection criterion $W_{sd} > 0.1(W - 0.3)$ (colour figure online)

Table 3 List of performance of the CTD-attached FP07 measurements and dependence on data rejection criteria from (a) to (e) at Station C04

Rejection Criterion	(1) Rejection rate of raw data (%)	(2) 10 m mean > 10 (%)	(3) 10 m mean σ(log)	(4) 50 m mean > 10 (%)	(5) 50 m mean σ(log)
(a) No W Wsd limit	0.00	48.10	1.28	73.17	1.15
(b) Wsd > 0.2 W-0.06	43.19	12.73	0.67	9.27	0.72
(c) Wsd > 0.1 W-0.02	57.80	10.32	0.76	6.34	0.68
(d) Wsd > 0.1 W-0.03	63.76	9.73	0.77	2.93	0.61
(e) Wsd > 0.1 W-0.04	69.72	10.26	0.78	2.93	0.61

(1) Rate of raw data rejection in % of total 8199 raw data; (2) rate of overestimated (> 10 of ε_S) data for 10 m mean in % out of 998 data; (3) the standard deviation σ(log) of 10 m mean $\log_{10}(\varepsilon_{TC}/\varepsilon_S)$ (ε_{TC}: from CTD-attached FP07 and ε_S: from VMP6000 shear); (4) same as (2) except for 50 m mean in % out of 205 data; (5) same as (3) except for 50 m mean. The σ(log) should be < 0.96 for 10 m mean and < 0.61 for 50 m mean (Goto et al. 2018)

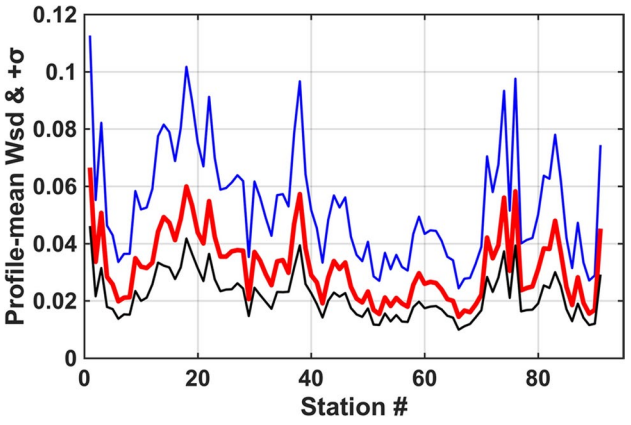

Fig. 8 Cast-mean fall speed variability cast mean-W_{sd} (red curve), standard deviation σ of W_{sd} in each cast (black) and the mean-$W_{sd}+\sigma$ (blue) at 91 CTD stations where each cast went to near-bottom along 137°E in the JMA-Ryofu-Maru RF1606 cruise to show W_{sd} under various sea-states (colour figure online)

data [< 3% (10) for 50 m (10) mean] and similar reasonable standard deviation of $\log_{10}(\varepsilon_{TC}/\varepsilon_S)$ (< 0.61 (0.77)% for 50 m (10) mean) with greater remaining raw data, $W_{sd} > 0.1(W-0.3)$ (Table 3d) may be better criterion for the rough conditions at Station C04 as also shown in the vertical profiles in Fig. 7c, d.

Even though the new criterion $W_{sd} > 0.1(W-0.3)$ was obtained in the present study for the rough sea condition without constant cable feeding winch system, we need to be careful. Disturbance from nearby instruments and CTD-frame, which depends on the configuration of the CTD-frame as well as sea state, may cause overestimated data. GYN18 and Goto et al. (2020) found such disturbance appeared at around small W and large W_{sd}, and near the minimum W. This is probably because a descending CTD frame and attached instruments drag adjacent water and generate turbulent wake, usually above the frame and instruments on the downstream side. On the other hand, when the CTD package decelerates more rapidly than the wake, which has downward momentum, the wake may be sampled at lowered W (GYN18). This issue needs to be further explored.

5 Conclusion

Observations of the turbulent energy dissipation rate, ε, using a fast-response thermistor FP07 were found to be useful at least down to $\varepsilon_T \sim 10^{-11}$ W/kg and for the Buoyancy Reynolds Number $R_{eB} > O(10)$ by comparing with shear probe measured ε_S using the free-fall VMP6000. $\varepsilon_T \sim \varepsilon_S$ estimated under the assumption of isotropic turbulence holds for $R_{eB} > 1$ and for $10^{-11} < \varepsilon_{T6} < 10^{-7}$ W/kg. This extends the observational range to $\varepsilon_{TC}=10^{-11}$–$10^{-8}$ W/kg by the CTD-attached FP07 observation from $\varepsilon_{TC}=10^{-10}$–$10^{-8}$ W/kg in previous studies (GYN18) where a less accurate smaller and tethered instrument of VMP2000 were used. This extension makes it much easier to take measurements of weak turbulence in deep oceans where $\varepsilon < 10^{-10}$ W/kg is prevalent. In such instance, this had previously been measured with a very scarce and expensive VMP and ship-time. It is noted that FP07 measurements are appropriate for such deep ocean measurements because probe-dependent time constants (but within 0–4 ms for double pole, within 0–10 ms for single-pole correction) of each FP07 probe do not affect ε_T for the relatively weak turbulence of $\varepsilon < 10^{-9}$ W/kg (GYN16). Although GYN18 demonstrated a method to obtain qualified data by rejecting questionable data using the $W_{sd} > 0.2(W-0.3)$ criterion, where the 1 s mean lowering rate is W and its standard deviation is W_{sd}. This study demonstrates that a stricter criterion, $W_{sd} > 0.1(W-0.3)$, is appropriate for a large lowering rate variability with the cast-mean $W_{sd} > 0.07$ m/s and its standard deviation of $\sigma > 0.05$ m/s. This FP07 method may be applied to mooring (e.g. Moum and Nash 2009) and profiling floats (R. Lien and E. Kunze, personal comm.).

Acknowledgements The authors thank anonymous reviews to improve the manuscript. Authors also thank the captain, officers, and crews of the R/V Shinsei-Maru and R/V Ryofu-Maru. This study is partially supported by KAKENHI JP15H05818/JPH05817/JP15K21710/JP20H05598.

Appendix

See Fig. 9.

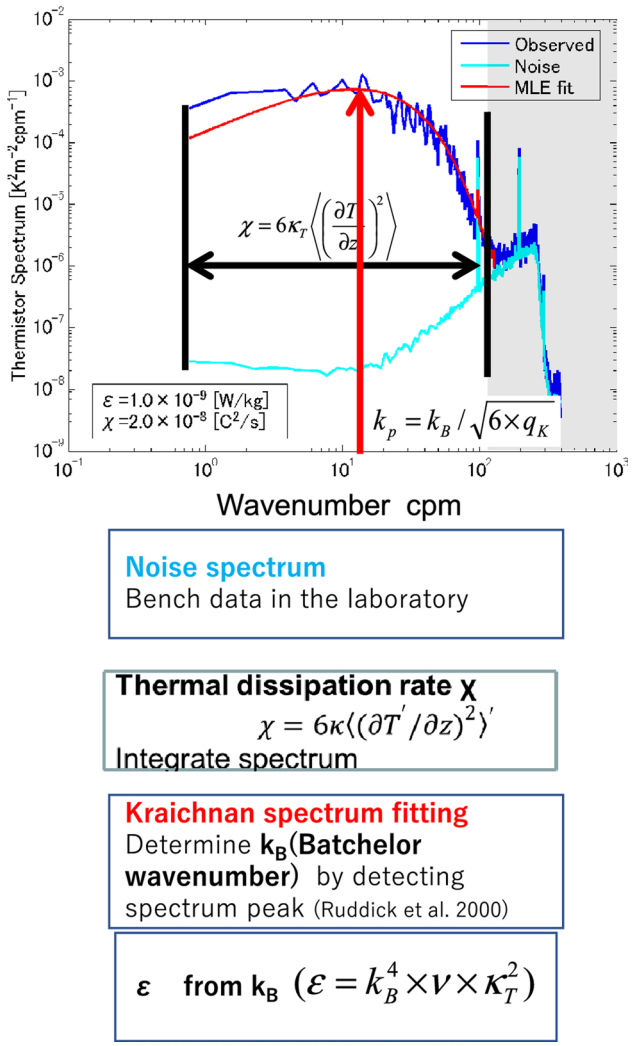

Fig. 9 Example of wavenumber-temperature gradient spectra and ε estimate from the observed spectrum (blue curve). This was undertaken by fitting the Kraichnan theoretical spectrum (red) and detecting the peak wavenumber, k_P, (red vertical arrow) proportional to the Batchelor wavenumber, k_B, to yield $\varepsilon(= k_B^4 \nu \kappa^2)$ through the estimate of the thermal dissipation rate, χ, by integrating the observed spectrum in the wavenumber range (black arrow) determined by the noise spectrum (light-blue) (colour figure online)

References

Batchelor GK (1959) Small-scale variation of convected quantities like temperature in turbulent fluid Part 1. general discussion and the case of small conductivity. J Fluid Mech 5:113–133. https://doi.org/10.1017/S002211205900009X

Becherer J, Moum JN (2017) An efficient scheme for onboard reduction of moored χ pod data. J Atmos Ocean Technol 34:2533–2546

Bogucki D, Domaradzki JA, Yeung PK (1997) Direct numerical simulations of passive scalars with Pr > 1 advected by turbulent flow. J Fluid Mech 343:111–130. https://doi.org/10.1017/S0022112097005727

Bogucki DJ, Luo H, Domaradzki JA (2012) Experimental evidence of the Kraichnan scalar spectrum at high Reynolds numbers. J Phys Oceanogr 42:1717–1728. https://doi.org/10.1175/JPO-D-11-0214.1

Bryan FO (1987) Parameter sensitivity of primitive equation ocean general circulation models. J Phys Ocean 17:970–985

Cox C, Nagata Y, Osborn T (1969) Oceanic fine structure and internal waves. Bulletin of the Japanese Society of Fisheries and Oceanography. Special Issue: Prof. Uda's Commemorative Papers, 67–71

Dillon TM, Caldwell DR (1980) The Batchelor spectrum and dissipation in the upper ocean. J Geophys Res 85:1910–1916. https://doi.org/10.1029/JC085iC04p01910

Gargett AE, Osborn TR, Nasmyth PW (1984) Local isotropy and the decay of turbulence in a stratified fluid. J Fluid Mech 144:231–280

Goodman L, Levine E, Lueck R (2006) On closing turbulence budgets from an AUV. J Atoms Ocean Tech 23:977–990

Goto Y, Yasuda I, Nagasawa M (2016) Turbulence estimation using fast-response thermistors attached to a free-fall vertical microstructure profiler. J Atmos Ocean Technol 33:2065–2078. https://doi.org/10.1175/JTECH-D-15-0220.1

Goto Y, Yasuda I, Nagasawa M (2018) Comparison of turbulence intensity from CTD-attached and free-fall microstructure profilers. J Atmos Ocean Technol 35:147–162. https://doi.org/10.1175/JTECH-D-17-0069.1

Goto Y (2018) Development and application of turbulence estimation using a fast-response thermistor attached to a CTD frame. Dissertation, University of Tokyo, pp 121

Goto Y, Yasuda I, Nagasawa M, Kouketsu S, and Nakano T (2020) Estimation of Basin-scale turbulence distribution in the North Pacific Ocean using CTD-attached thermistor measurements. Sci Rep. https://doi.org/10.1038/s41598-020-80029-2

Gregg MC (1999) Uncertainties and limitations in measuring ε and χT. J Atmos Ocean Technol 16:1483–1490

Gregg MC, Meagher TB (1980) The dynamic response of glass rod thermistors. J Geophys Res 85:2779–2786. https://doi.org/10.1029/JC085iC05p02779

Gregg MC, Meagher TB, Pederson A, Aagaard E (1978) Low noise temperature microstructure measurements with thermistors. Deep-Sea Res 25:843–856

Hasumi H, Yasuda I, Tatebe H, Kimoto M (2008) Pacific bidecadal climate variability regulated by tidal mixing around the Kuril Islands. Geophys Res Lett 35:L14601. https://doi.org/10.1029/2008GL034406

Kaneko H, Yasuda I, Komatsu K, Itoh S (2013) Observations of vertical turbulent nitrate flux across the Kuroshio. Geophys Res Lett 40(12):3123–3127

Kobari T, Honma T, Hasegawa D et al (2020) Phytoplankton growth and consumption by microzooplankton stimulated by turbulent nitrate flux suggest rapid trophic transfer in the oligotrophic Kuroshio. Biogeosciences 17:2441–2452. https://doi.org/10.5194/bg-17-2441-2020

Kraichnan RH (1968) Small-scale structure of a scalar field convected by turbulence. Phys Fluids 11:945–953. https://doi.org/10.1063/1.1692063

Lueck RG, Hertzman O, Osborn TR (1977) The spectral response of thermistors. Deep-Sea Res 24:951–970. https://doi.org/10.1016/0146-6291(77)90565-3

Lueck RG, Wolk F, Yamazaki H (2002) Oceanic velocity microstructure measurements in the 20th century. J Oceanogr 58:153–174. https://doi.org/10.1023/A:1015837020019

Moum JN, Nash JD (2009) Mixing measurements on an equatorial ocean mooring. J Atmos Oceanic Technol 26:317–336. https://doi.org/10.1175/2008JTECHO617.1

Mudge TD, Lueck RG (1994) Digital signal processing to enhance oceanographic observations. J Atmos Ocean Technol 13:825–836

Munk WH (1966) Abyssal recipes. Deep-Sea Res 13(4):707–730

Nasmyth PW (1970) Oceanic turbulence. Dissertation, University of British Columbia

Nishioka J, Obata H, Ozawa H, Ono K, Yamashita Y, Lee KJ, Takeda S, Yasuda I (2020) Sub-polar marginal seas fuel the North Pacific through the intermediate water at the termination of the global ocean circulation. Proc Natl Acad Sci USA 117(23):12665–12673. https://doi.org/10.1073/pnas.2000658117

Oakey NS (1982) Determination of the rate of dissipation of turbulent energy from simultaneous temperature and velocity shear microstructure measurements. J Phys Ocean 12(3):256–271

Oka A, Niwa Y (2013) Pacific deep circulation and ventilation controlled by tidal mixing away from the sea bottom. Nat Commun 4:2419

Osborn TR (1980) Estimates of the local rate of vertical diffusion from dissipation measurements. J Phys Oceanogr 10:83–89

Osborn TR, Cox CS (1972) Oceanic fine structure. Geophys Fluid Dyn 3:321–345

Ozmidov RV (1965) On the turbulent exchange in a stably stratified ocean. Izv Acad Sci USSR Atmos Oceanic Phys 1:861–871

Peterson AK, Fer I (2014) Dissipation measurements using temperature microstructure from an underwater glider. Methods Ocean 10:44–69. https://doi.org/10.1016/j.mio.2014.05.002

Ruddick B, Anis A, Thompson K (2000) Maximum likelihood spectral fitting: the Batchelor spectrum. J Atmos Ocean Technol 17:1541–1555. https://doi.org/10.1175/1520-0426(2000)017%3c1541:MLSFTB%3e2.0.CO;2

Scheifele B, Waterman S, Merckelbach L, Carpenter JR (2018) Measuring the dissipation rate of turbulent kinetic energy in strongly stratified, low-energy environments: a case study from the Arctic Ocean. J Geophys Res Oceans 123:5459–5480. https://doi.org/10.1029/2017JC013731

Tanaka Y, Yasuda I, Hasumi H, Tatebe H, Osafune S (2012) Effects of the 18.6-yr modulation of tidal mixing on the North Pacific bidecadal climate variability in a coupled climate model. J Clim 25(21):7625–7642

Tanaka T, Yasuda I, Kuma K, Nishioka J (2012) Vertical turbulent iron flux sustains the Green Belt along the shelf break in the southeastern Bering Sea. Res. Lett, Geophys. https://doi.org/10.1029/2012GL051164

Tanaka M, Yoshida J, Lee KJ, Goto Y, Tanaka T, Ueno H, Onishi U, Yasuda I (2020) The potential role of thermohaline-shear instability in turbulence production. J Oceanogr (**in revision**)

Tatebe H, Tanaka Y, Komuro Y et al (2018) Impact of deep ocean mixing on the climatic mean state in the Southern Ocean. Sci Rep 8:14479. https://doi.org/10.1038/s41598-018-32768-6

Watanabe M, Tatebe H, Suzuki T, Tachiiri K (2020) Control of transient climate response and associated sea level rise by deep-ocean mixing. Environ Res Lett 15(2020):094001. https://doi.org/10.1088/1748-9326/ab8ca7

Waterhouse AF et al (2015) Global patterns of diapycnal mixing from measurements of the turbulent dissipation rate. J Phys Oceanogr 44(7):1854–1872

Yamazaki H, Osborn TP (1990) Dissipation estimates for stratified turbulence. J Geophys Res 95:9739–9744. https://doi.org/10.1029/JC095iC06p09739

Yasuda I (2009) The 18.6-year period moon-tidal cycle in Pacific Decadal Oscillation reconstructed from tree-rings in western North America. Geophys Res Lett 36:L05605. https://doi.org/10.1029/2008GL036880

Yasuda I (2018) Impact of the astronomical lunar 18.6-yr tidal cycle on El-Niño and Southern Oscillation. Sci Rep 8:15206. https://doi.org/10.1038/s41598-018-33526-4

Yasuda I, Osafune S, Tatebe H (2006) Possible explanation linking 18.6-year period nodal tidal cycle with bi-decadal variations of ocean and climate in the North Pacific. Geophys Res Lett 33:L08606. https://doi.org/10.1029/2005GL025237